



Investigation of Structural and Acoustic Responses of a Submerged Cylindrical Enclosure under Arbitrary Force Excitations

Xia Pan, Ian MacGillivray and James Forrest

Maritime Division, Defence Science and Technology Group, Victoria, Australia

ABSTRACT

This paper models and analyses the structural behaviour and radiated sound due to arbitrary force excitations of a cylindrical enclosure totally submerged in a heavy fluid. The enclosure consists of a cylindrical shell with internal bulkheads and ring stiffeners. The cylindrical shell is closed by circular plates. The structural responses of the shell and plates are calculated by solving the shell and plate equations of motion using a wave approach. The far-field radiated sound pressure from the shell and plates is then calculated by using the Helmholtz integral. The effect on the vibration and far-field sound pressure of the whole enclosure resulting from arbitrary force excitations is investigated. The influence of the bulkheads and ring stiffeners on the structure is discussed. Good agreement is obtained between the analytical results and results from numerical finite element / boundary element models.

1 INTRODUCTION

In naval applications, it is important to be able to estimate the noise radiated underwater by a vibrating hull structure under arbitrary force excitations during its design stage. Submerged cylindrical enclosures may be used as simple examples to demonstrate the structural and acoustic characteristics of underwater vessels. This paper analytically and numerically investigates the vibration and sound radiation from a cylindrical enclosure due to arbitrary force excitations.

Structural vibration and sound radiation from a submerged cylindrical enclosure can be modelled analytically using the following three steps. The first step is to model the structural responses of a finite cylindrical shell and a finite plate. Detailed discussions and comparisons of different shell equations and general solutions were given by Pan and Hansen (1997) and Caresta and Kessissoglou (2009). The plate equations and general solutions of bending and in-plane motions of a circular plate were described by Tso and Hansen (1995). The coupling of the shell and plates is then applied to the boundary between the shell and plates. The second step is to model the excitations. The expression for a point force acting on a shell in the radial or axial direction has been reported (see, for example, Pan and Hansen 1997 for a radial force and Caresta and Kessissoglou 2009 for an axial force). However, only limited work has been published on analytical studies for a tangential force acting on a shell. Laulagnet and Guyader (1990) conducted an analytical study of radiation by a simply supported, stiffened shell. They applied a radial, axial or tangential force on the stiffener and found that the radial and tangential forces produced similar velocity and power levels below the ring frequency. The expressions for a point force acting on a plate have been commonly limited to a transverse force (Tso and Hansen 1995 and Skelton and James 1997). The third step is to model the sound radiation from the shell and end plates. An approximation for sound radiation from a vibrating shell was given by Junger and Feit (1986) and used in Pan *et al.* (2008a, 2008b) based on the spectral radial shell displacement. An approximation for sound radiation from an infinite plate was given by Skelton and James (1997) based on the spectral normal plate displacement.

Sound radiation from a submerged hull modelled using a fully coupled finite element / boundary element (FE/BE) method was reported by Peters *et al.* (2014). They applied uniform vertical, transverse and axial excitations on the hull and found that the peaks of radiated sound were primarily due to the beam bending mode $n = 1$ of the hull for the vertical and transverse excitations. Their method was validated by Qu *et al.* (2015) using a semi-analytical method.

The work described here is an extension of previous work (Caresta and Kessissoglou 2009) on the total sound radiation from a free cylindrical enclosure due to arbitrary point axial force excitation. The enclosure includes a cylindrical shell and two end plates. Sound radiation from the finite shell, finite end plates and the entire enclosure is respectively given in the current paper. An arbitrary force can be decomposed into three orthogonal forces. The three orthogonal forces used here are in the radial, axial and tangential directions and are applied to the edge of

the shell on the shell-plate boundary. The results of the sound radiation obtained from the analytical models are validated against those obtained from numerical FE/BE models using the software Sysnoise.

2 THEORETICAL METHOD

2.1 Dynamic Model of the Submerged Cylindrical Enclosure

The cylindrical enclosure consists of a finite ring-stiffened cylindrical shell closed at each end by a circular plate. The shell is partitioned into three parts by two equally spaced bulkheads. The ring stiffeners are modelled using smeared theory (Hoppmann 1958). In Figure 1, u, v and w are the axial, tangential and radial displacements on the shell, a is the mean radius of the shell and h is the shell thickness.

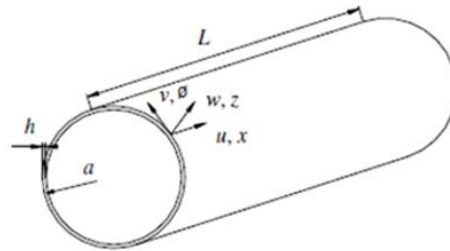


Figure 1: Coordinate system and displacements for a thin cylindrical shell

The equations of motion using the Flügge theory for a ring-stiffened cylindrical shell were given by Rosen and Singer (1974), and can be written in terms of differential operators L_{ij} as

$$L_{11}u + L_{12}v + L_{13}w = 0, \quad L_{21}u + L_{22}v + L_{23}w = 0, \quad L_{31}u + L_{32}v + L_{33}w - \frac{p_a}{\rho h c_L^2} = 0, \quad (1a-1c)$$

where p_a is the external pressure loading due to the fluid reacting on the structure and ρ and c_L are respectively the density and longitudinal wave speed of the shell (see Scott 1998 and Caresta and Kessissoglou 2009).

The general solutions to Equations (1) due to the axial and radial forces (refer to Figure 3 below) can be written as the double Fourier series

$$u = \sum_{n=0}^{\infty} \sum_{i=1}^8 C_{n,i} W_{n,i} e^{jk_n i x} \cos(n \varnothing) e^{-j\omega t} \quad (2a)$$

$$v = \sum_{n=0}^{\infty} \sum_{i=1}^8 G_{n,i} W_{n,i} e^{jk_n i x} \sin(n \varnothing) e^{-j\omega t} \quad (2b)$$

$$w = \sum_{n=0}^{\infty} \sum_{i=1}^8 W_{n,i} e^{jk_n i x} \cos(n \varnothing) e^{-j\omega t} \quad (2c)$$

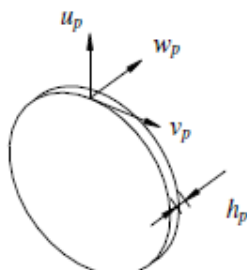
where $C_{n,i} = U_{n,i}/W_{n,i}$, $G_{n,i} = V_{n,i}/W_{n,i}$, k_n is the axial wavenumber and n is the circumferential mode number. The expression for the general solutions due to the tangential force excitation may be obtained by changing the solution of the tangential displacement (Equation (2b)) to an even function around the central line of the shell. This can be done by swapping $\sin(n \varnothing)$ and $\cos(n \varnothing)$ in Equations (2a) to (2c) which can then be written as

$$u = \sum_{n=0}^{\infty} \sum_{i=1}^8 C_{n,i} W_{n,i} e^{jk_n i x} \sin(n \varnothing) e^{-j\omega t} \quad (3a)$$

$$v = \sum_{n=0}^{\infty} \sum_{i=1}^8 G_{n,i} W_{n,i} e^{jk_n i x} \cos(n \varnothing) e^{-j\omega t} \quad (3b)$$

$$w = \sum_{n=0}^{\infty} \sum_{i=1}^8 W_{n,i} e^{jk_n i x} \sin(n \varnothing) e^{-j\omega t}. \quad (3c)$$

The end plates and bulkheads are modelled as thin circular plates in bending and in-plane motion. In Figure 2, u_p , v_p and w_p are the axial, tangential and radial displacements on the plates and h_p is the plate thickness.



Source (Caresta and Kessissoglou, 2009)
Figure 2: Displacements for a thin circular plate

Displacements for the plates and bulkheads due to the axial and radial force excitations were given by Tso and Hansen (1995) as

$$u_p = \sum_{n=0}^{\infty} (B_{n,1} \frac{\partial J_n(k_{pL}a)}{\partial a} + \frac{nB_{n,2} J_n(k_{pT}a)}{a}) \cos(n\phi) e^{-j\omega t} \quad (4a)$$

$$v_p = - \sum_{n=0}^{\infty} (\frac{nB_{n,1} J_n(k_{pL}a)}{a} + B_{n,2} \frac{\partial J_n(k_{pT}a)}{\partial a}) \sin(n\phi) e^{-j\omega t} \quad (4b)$$

$$w_p = \sum_{n=0}^{\infty} (A_{n,1} J_n(k_{pB}a) + A_{n,2} I_n(k_{pB}a)) \cos(n\phi) e^{-j\omega t} \quad (4c)$$

where $A_{n,i}$ and $B_{n,i}$ ($i = 1, 2$) are constants defined below, k_{pB} is the plate bending wavenumber and k_{pT} and k_{pL} are the wavenumbers for in-plane waves in the plate (Tso and Hansen 1995). J_n and I_n are respectively Bessel functions and modified Bessel functions of the first kind.

The expression for the displacement of the plates due to the tangential force may be written as

$$u_p = \sum_{n=0}^{\infty} (B_{n,1} \frac{\partial J_n(k_{pL}a)}{\partial a} + \frac{nB_{n,2} J_n(k_{pT}a)}{a}) \sin(n\phi) e^{-j\omega t} \quad (5a)$$

$$v_p = - \sum_{n=0}^{\infty} (\frac{nB_{n,1} J_n(k_{pL}a)}{a} + B_{n,2} \frac{\partial J_n(k_{pT}a)}{\partial a}) \cos(n\phi) e^{-j\omega t} \quad (5b)$$

$$w_p = \sum_{n=0}^{\infty} (A_{n,1} J_n(k_{pB}a) + A_{n,2} I_n(k_{pB}a)) \sin(n\phi) e^{-j\omega t}. \quad (5c)$$

2.2 Arbitrary point forces

Four excitation cases are presented in Figure 3. F_c is an axial point force applied to the center of the circular plate at $x = 0$. For numerical reasons, this was dynamically modelled by separating the circular plate into an inner circular plate over very small radius and outer annular plate. The point force at the center of the plate was then approximated as a distributed force applied axially at the junction of the annular and inner circular plates. The excitation gives rise to an axisymmetric case corresponding to excitation of the shell zeroth modes $n = 0$. F_a , F_t and F_r are the axial, tangential and radial forces applied to the edge of the cylindrical shell at one end. Any arbitrary point force can be decomposed into these three orthogonal components; an arbitrary end force distribution can be represented as a linear combination of such point forces around the circumference. A point force located at $(x_0, \phi_0) = (0, 0)$ is described in terms of Dirac delta functions by

$$F(x, \phi, t) = F_0 \delta(x - x_0) \delta(\phi - \phi_0) e^{-j\omega t} = F_0 \delta(x) \delta(\phi) e^{-j\omega t}. \quad (6)$$

Rotational symmetry means responses to this force would be the same as responses to forces in other circumferential positions with an appropriate angular shift. This might be useful to increase computational efficiency for more complicated force distributions beyond the single point force cases considered in this paper.

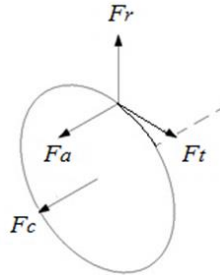


Figure 3: Four excitation cases at the end plate and edge of the cylindrical shell

2.3 Radial displacements of the shell and end plates

For each value of n , the shell wavenumbers k_n are determined by substituting the general solutions into the equations of motion of the shell, solving for determinant equal to zero, and then adding fluid loading by introducing both mass and damping effects as done by Caresta and Kessissoglou (2009). The plate wavenumbers k_{pB} , k_{pT} and k_{pL} depend only on frequency and plate parameters (Tso and Hansen 1995). Only the cylindrical shell is fully coupled to the surrounding water.

The dynamic response of the submerged cylindrical enclosure is expressed in terms of $A_{n,i}$ and $B_{n,i}$ ($i = 1, 2$) for each circular plate and $W_{n,i}$ ($i = 1:8$) for each section of the shell. The whole structure consists of three cylindrical shell segments and four circular plates, thus there are 40 unknown displacement coefficients for the shell segments, bulkheads and end plates. A schematic diagram of the modelled hull is shown in Figure 4.

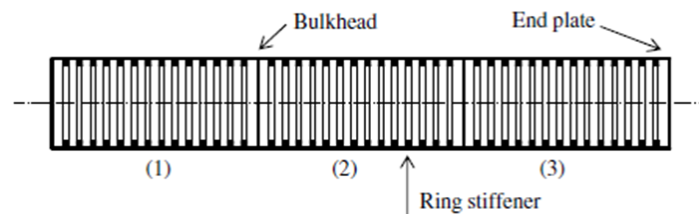


Figure 4: Schematic diagram of cylindrical enclosure

The entire enclosure has no boundary condition constraints. At the cylindrical shell and plate junctions, continuity of displacements and equilibrium of forces / moments have to be satisfied. The boundary and continuity equations can be arranged in matrix form $\alpha X = F$, where X is the vector of the unknown displacement coefficients and F is the vector containing the external point force terms. Each of the four point forces as described in Section 2.2 is placed in F containing only one non-zero term corresponding to either $\varepsilon F_0 \cos(n\phi_0)$ or $\varepsilon F_0 \sin(n\phi_0)$ ($\varepsilon = 1/2\pi a$ if $n = 0$ and $\varepsilon = 1/\pi a$ if $n \neq 0$). For a point force located at $(x_0, \phi_0) = (0, 0)$, the force component reduces to εF_0 . Once the unknown coefficients have been determined, the radial displacements of the shell and end plates can be obtained. The radial displacements are then used for calculating the far-field sound pressure as shown below.

2.4 Far-field sound pressure from the shell and end plates

The definition of the coordinate system, for the field point at which the pressure from the cylindrical shell and end plates is computed, is shown in Figure 5.

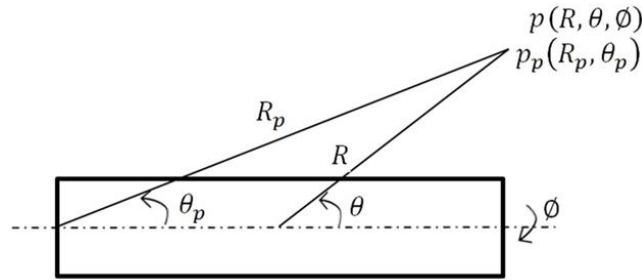


Figure 5: Definition of the coordinate system for the field point

If the axial or radial force is applied on the shell, the sound pressure in the far-field is given by Junger and Feit (1986) as

$$p(R, \theta, \phi) = \frac{\rho_f \omega^2 e^{jk_f R}}{\pi k_f R \sin \theta} \sum_{n=0}^{\infty} \frac{(-j)^{n+1} \hat{w}_n(k_f \cos \theta)}{H'_n(k_f a \sin \theta)} \cos(n \phi) \quad (7)$$

where ρ_f is the fluid density, k_f is the fluid wavenumber, H_n is the Hankel function of order n and $\hat{w}_n(k_f \cos \theta)$ is defined as

$$\hat{w}_n(k_f \cos \theta) = \sum_{i=1}^8 \int_{-L/2}^{L/2} W_{n,i} e^{jk_{n,i} x} e^{-jk_f \cos \theta x} dx \quad (8)$$

where $W_{n,i}$ is the modal radial displacement amplitude for the i^{th} axial wavenumber at the circumferential mode n as shown in Equation (2c).

If the tangential force is applied on the shell, the expression for the pressure is obtained by swapping $\cos(n \phi)$ for $\sin(n \phi)$ in Equation (7) as

$$p(R, \theta, \phi) = \frac{\rho_f \omega^2 e^{jk_f R}}{\pi k_f R \sin \theta} \sum_{n=0}^{\infty} \frac{(-j)^{n+1} \hat{w}(k_f \cos \theta)}{H'_n(k_f a \sin \theta)} \sin(n \phi) \quad (9)$$

where $\hat{w}(k_f \cos \theta)$ can be obtained similarly using the radial displacement amplitude due to the tangential force excitation (Equation (3c)).

For a finite plate, the far-field pressure at low frequencies can be developed by modifying the pressure from an infinite plate (Skelton and James 1997) as

$$p_p(R_p, \theta_p) = -\rho_f \omega^2 \hat{w}_p \frac{e^{jk_f R_p}}{4\pi R_p} \quad (10)$$

where \hat{w}_p is the integral transform of the radial displacement of the finite plate. For a finite circular plate, \hat{w}_p was approximated by McLachlan (1954) as

$$\hat{w}_p = \int_0^a \int_0^{2\pi} w_p e^{-jk_f r \sin \theta_p \cos \phi_1} r dr d\phi_1 \quad (11)$$

where w_p is the plate radial displacement corresponding to the force type. Substituting Equation (11) into Equation (10), the far-field pressure from a circular plate can be obtained.

The total pressure from the entire cylindrical enclosure can be obtained by summing the pressure from the shell and the two end plates.

3 NUMERICAL METHOD

The numerical FE/BE modelling was performed using a combination of the commercial software packages ANSYS and Sysnoise using a three-stage process. In the first stage the physical structure of the cylinder and end plates was built within ANSYS. A finite element modal analysis of the unconstrained cylinder in-vacuo was then obtained using the Sysnoise FEM structural module.

For the second stage, the modal basis set was used in a fully coupled direct boundary-element calculation within Sysnoise. Although the analytical model described in section 2 uses a cylinder fully coupled to the surrounding water, the end plate theory does not couple the end plates to water. In order to match the physics of the analytical theory with the numerical model, the water loading on the cylinder within Sysnoise was only applied to the cylinder and not to the end plates. Coupled modes for such water loading were then generated and the frequency-dependent displacements of the structure saved for acoustic radiation modelling.

In the third stage, the vibration of the cylinder and end plates were used as vibration boundary conditions within Sysnoise to compute separately the contribution to radiated pressure of the plates and cylinder with the cylinder fully immersed in water.

Material properties were as used in Section 4. The modal approach using Sysnoise is unable to directly use complex moduli but a modal loss factor of 2% was used for each coupled mode computed by Sysnoise. This was done in order to approximately match the loss factor for the analytical model.

Results presented here were obtained using 800 in-vacuo (uncoupled) modes, corresponding to frequencies up to 196 Hz, with a mesh consisting of 18000 elements. Note that these modes do not directly relate to the circumferential “mode” numbers of the analytical model. Coupled modes for the water loading corresponded to wet frequencies up to 187 Hz. Computation times on a low-end workstation, for frequencies 0–100 Hz at 1 Hz intervals, were typically an hour for the uncoupled modes calculation, 70 hours for each forcing direction, and 10 hours each for the radiation calculation of both ends and cylinder. Lower resolution runs were also performed to check that the results were consistent, but as the physical model was large it was not possible to ensure that results to 100 Hz were truly independent of the resolution.

4 RESULTS

Unless otherwise indicated, the results presented in this paper are based on a ring-stiffened steel cylindrical enclosure of radius $a = 3.25$ m, shell and plate thickness $h = h_p = 0.04$ m, length $L = 45$ m and with two evenly spaced bulkheads of thickness $h_p = 0.04$ m. The material properties for steel are density $\rho = 7800$ kgm⁻³, Young’s modulus $E = 2.1 \times 10^{11}$ Nm⁻² and Poisson’s ratio $\nu = 0.3$. The internal stiffeners have a rectangular cross section of 0.08×0.15 m² and are evenly spaced by 0.5 m. Damping in the shell and plates is included by using a complex representation of the Young’s modulus $E = E(1 - j\eta)$, where η is the loss factor and has a value of 0.02. All results are normalized to be per unit force. The sound pressure was calculated at 1000 m with $\theta = 90^\circ$ and $\phi = 0^\circ, 90^\circ$, and normalized to 1 m range by adding 60 dB. The pressure dB reference level is 1 μ Pa.

4.1 Analytical results

Since the $n \geq 2$ circumferential modes are not efficient sound radiators (Caresta and Kessissoglou 2009, Peters *et al.* 2014 and Qu *et al.* 2015), only the $n = 0 - 3$ modes are considered in the analytical results.

The effect of the three orthogonal force excitations on the frequency response of displacement at the driving point without stiffeners and without bulkheads is presented in Figures 6(a) to 6(c). At the driving point, the circumferential angle is zero ($\phi = 0$). Figure 6(a) shows the radial displacement due to the radial and axial forces. The radial displacement due to the tangential force at the driving point is zero (see Equation 3(c)). The resonance peaks are labelled with the corresponding circumferential mode number n . The resonance peaks in Figure 6(a) correspond to the $n = 1$ mode, which corresponds to beam bending motion of the shell. Figure 6(b) presents the axial displacement due to the radial or axial force. The axial displacement due to the tangential force at the driving point is zero (see Equation 3(a)). The peaks in axial displacement due to the radial force correspond to the $n = 1$ mode. The peaks in the axial displacement due to the axial force are dominated by the $n = 0$ breathing mode and $n = 1$ bending mode, and only a few small peaks result from the $n = 2$ and $n = 3$ modes. Figure 6(c) shows the tangential displacement at the driving point due to the tangential force only as the tangential displacement due to the radial or axial force is zero (see Equation 2(b)). The peaks in Figure 6(c) correspond to the $n = 1$ mode. This may be because the tangential force causes the shell to deform in a beam torsional motion as well as beam bending (both correspond to $n = 1$ in their respective directions) i.e. the shell is twisting in the tangential force direction (see Figure 3), below the ring frequency at about 260 Hz (refer to Laulagnet and Guyader 1990).

The effect of the stiffeners on the dynamic response of the enclosure, as shown in Figure 6, is demonstrated by comparison with calculations with the stiffeners included. Figures 7(a) to 7(c) present the comparisons of the displacements shown in Figures 6(a) to 6(c) with those including the stiffeners respectively. It can be observed that the resonances of the stiffened cylindrical shell are slightly lower than those of the unstiffened shell at low frequencies, and are attributed to the mass added by the stiffeners. At higher frequencies, the resonance frequencies of the stiffened shell are slightly increased over those of the unstiffened shell, and this is attributed to a stiffening effect.

The effect of adding the bulkheads on the responses at the driving point is shown in Figures 8(a) to 8(c). Figure 8 shows the comparisons of the displacements calculated with and without the two bulkheads. It can be seen that the bulkheads do not significantly affect the dynamic response of the structure at the driving point.

The cylindrical enclosure includes a cylindrical shell and two end plates. Sound pressure from the shell and end plates is calculated separately, with the total pressure from the entire enclosure obtained by summing. The results of sound pressure shown in this section have been calculated for the enclosure without stiffeners and without bulkheads.

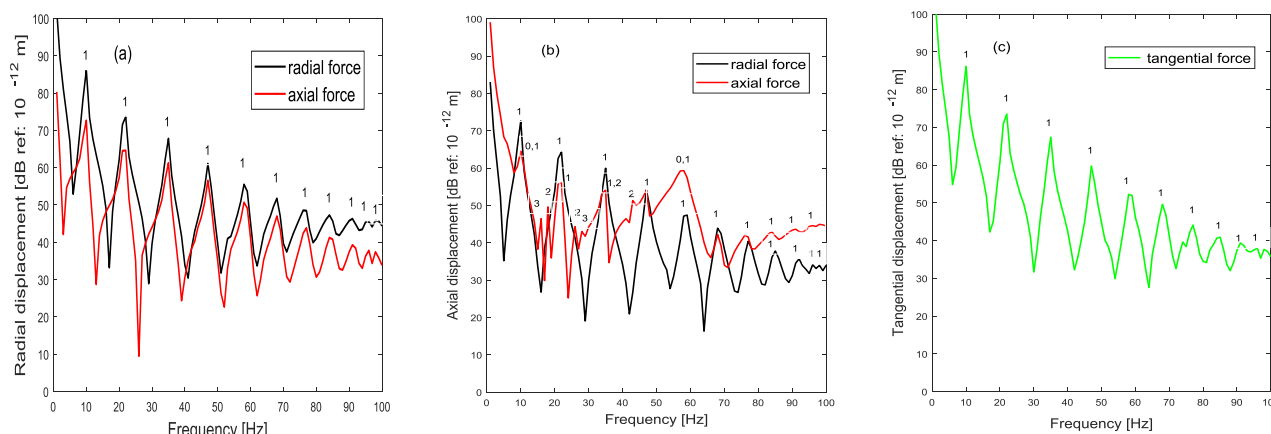


Figure 6: Frequency responses of displacements at the driving point due to three orthogonal forces without stiffeners and without bulkheads: (a) radial displacement; (b) axial displacement; (c) tangential displacement

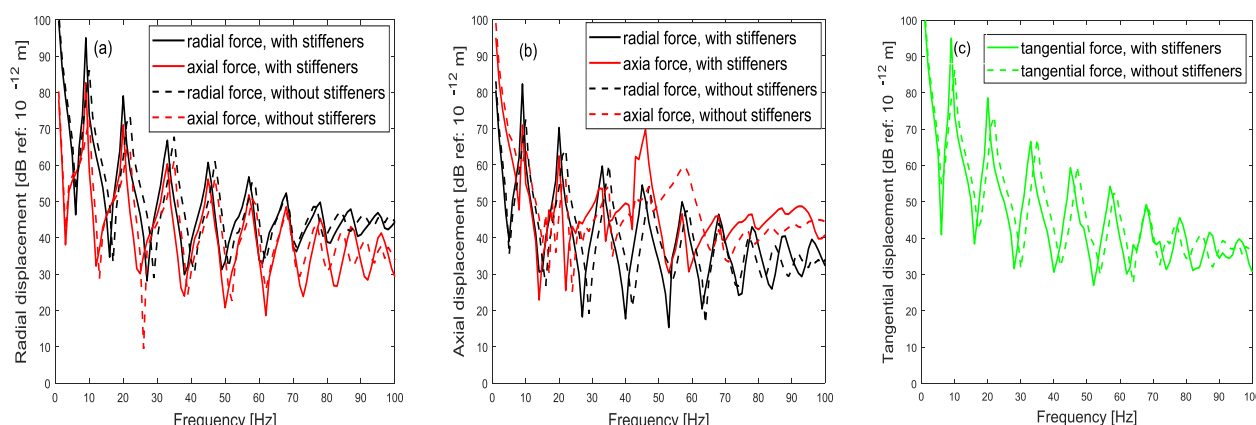


Figure 7: Frequency responses of displacements at the driving point with and without stiffeners: (a) radial displacement; (b) axial displacement; (c) tangential displacement

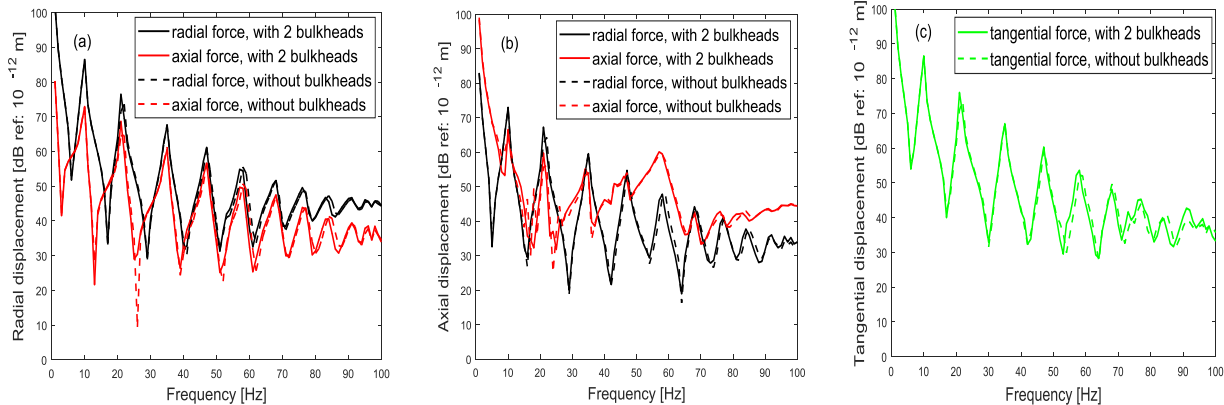


Figure 8: Frequency responses of displacements at the driving point with and without bulkheads: (a) radial displacement; (b) axial displacement; (c) tangential displacement

Figures 9(a) to 9(c) show the sound pressure obtained from individual parts of the enclosure and the entire enclosure due to the three orthogonal forces. The pressure was calculated at $\theta = 90^\circ$ and $\phi = 0^\circ$, which is on the same side of the cylinder as the driving force. Figure 9(a) shows the radiated pressure from the cylindrical shell due to radial and axial force excitations. The pressure due to the tangential force is zero (see Equation (9) with $\phi = 0$). In Figure 9(a), large peaks in the pressure due to the radial force are observed. A comparison has been made of the pressure from the shell due to the radial force for the bending mode only (i.e. $n = 1$ only; not given here). It was found they were similar. Thus, the peaks in the pressure are considered to correspond to the bending mode. This phenomenon is similar to that reported by Peters *et al.* (2014) using a fully coupled FE/BE method for a similar structure and excitation. The peaks in the pressure due to the axial force result from the breathing mode ($n = 0$) and bending mode by comparing the pressure with those for the individual modes. This confirms the finding of Caresta and Kessissoglou (2009). Figure 9(b) shows the pressure obtained from the two end plates. The plates radiate sound for each of the three forces, but the tangential force results in sound radiation about 40 dB lower than that for the axial force at most frequencies below 50 Hz. The reason the end plates slightly radiate sound due to a tangential force is because the shell is coupled with the plates. The offset tangential force can excite both tangential and radial motion in the shell; these motions couple to axial motion in the shell, which reacts on the plates to generate some plate normal motion and hence sound radiation. Note that the plate pressure due to the radial or tangential force is slightly higher than the pressure due to the axial force at some frequencies above 90 Hz, which may be related to the approximations in the analytical plate model. Comparing Figures 9(a) and 9(b), it can be seen that the pressure from the shell and the pressure from the end plates due to the axial force are both comparable. There are two reasons. Firstly, the shell and end plates are both flexible to radiate sound. Secondly, the axial force is normal to the end plates, exciting them efficiently under the axial force excitation. Figure 9(c) shows the pressure from the entire enclosure. The total pressure at this observation point due to the radial or axial force is much higher than that due to the tangential force.

Figures 10(a) to 10(c) present the pressure calculated at $\theta = 90^\circ$ and $\phi = 90^\circ$. In Figure 10(a), the pressure due to the tangential force is observed to be generally greater than the pressure due to the radial or axial force, as the observed pressure is located in the same direction as that of the tangential force. The peaks in the pressure due to the tangential force have been identified as corresponding to the bending mode by comparing with the pressure calculated using only the $n = 1$ mode (results not given here). This phenomenon is similar to that reported by Peters *et al.* (2014). Figure 10(c) shows that the total pressure due to the tangential force is generally higher than the total pressure due to the other two forces at this observation point. The results shown in Figures 10(a) to 10(c) indicate the effect of the tangential force on sound pressure can be significant at some observation points.

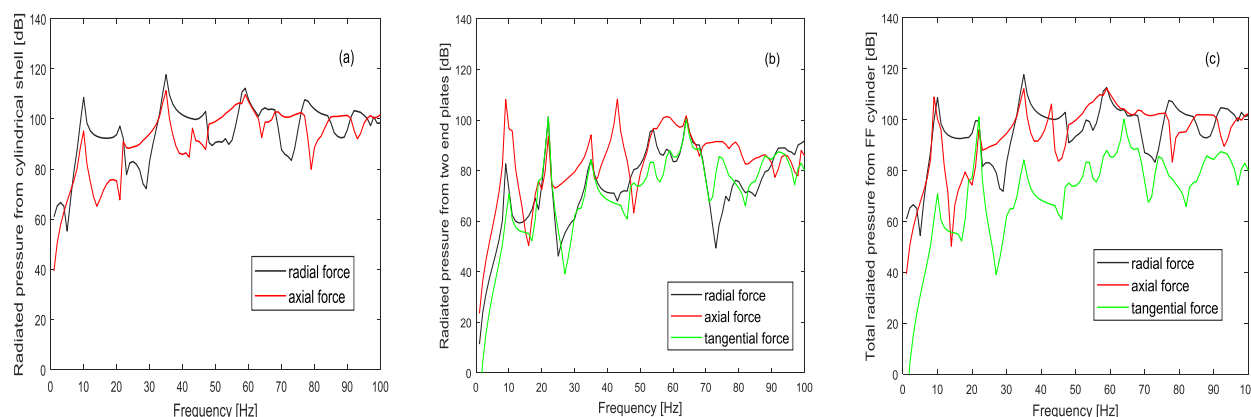


Figure 9: Sound pressure at $\theta = 90^\circ$ and $\phi = 0^\circ$ due to three orthogonal forces: (a) shell; (b) end plates; (c) entire enclosure

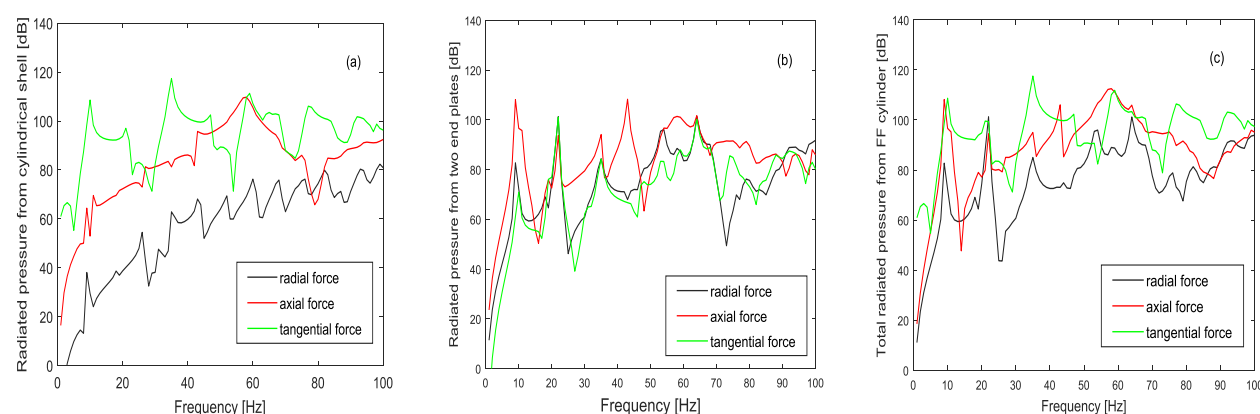


Figure 10: Sound pressure at $\theta = 90^\circ$ and $\phi = 90^\circ$ due to three orthogonal forces: (a) shell; (b) end plates; (c) entire enclosure

4.2 Comparison with numerical results

In this section, the Sysnoise method described in Section 3 is used to verify the analytical results. For an initial comparison, only the numerical results for the cylindrical enclosure without stiffeners and without bulkheads will be compared with those obtained from the analytical results.

Figures 11(a) to 11(c) compare the frequency responses of displacements at the driving point due to the three orthogonal forces obtained from the analytical and numerical models. Excellent agreement is obtained at low frequencies. As frequency increases, some differences between the two models are observed. This may be because the numerical calculation was not accurate enough at higher frequencies, but could also be related to approximations in the analytical model.

For the comparison of the far-field sound pressure, only the axisymmetric case is considered. In this case, the point force F_c is applied at the center of the plate as shown in Figure 3. Only the breathing mode $n = 0$ of the shell can be generated. Figures 12 (a) to 12(c) present, respectively, the far-field sound pressure from the cylindrical shell, end plates and entire enclosure. Excellent agreement is obtained between the analytical results and the results from the numerical method.

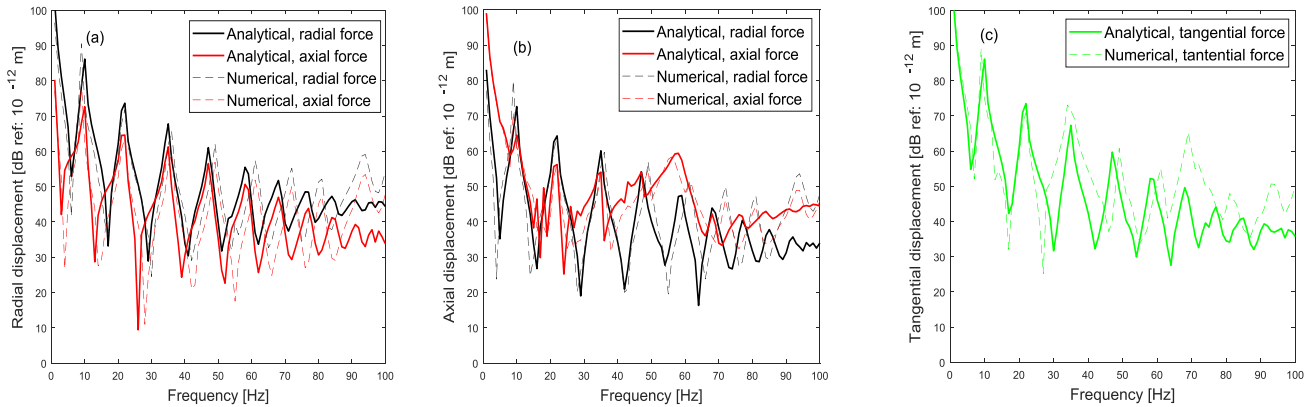


Figure 11: Comparison of analytical and numerical frequency responses of displacements at the driving point due to three orthogonal forces: (a) radial displacement; (b) axial displacement; (c) tangential displacement

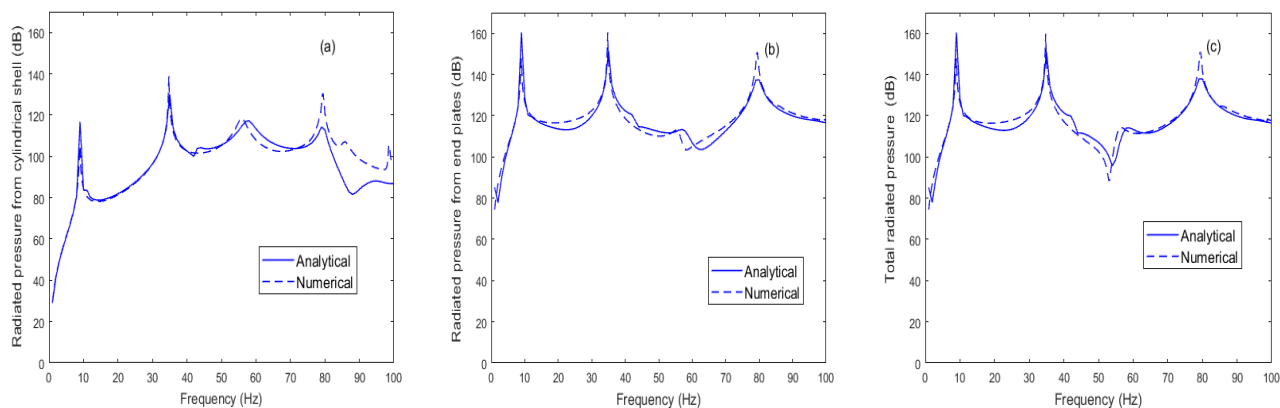


Figure 12: Comparison of analytical and numerical sound pressure due to an axial force applied to the centre of an end plate: (a) shell; (b) end plates; (c) entire enclosure

5 DISCUSSION

Issues relating to comparison of the analytical and numerical results will be discussed in this section. The importance of the bending mode of the shell on the far-field sound pressure was observed in the analytical results. The analytical results indicated that the resonance peaks in the pressure resulting from the radial or tangential force were primarily corresponding to the bending mode. The numerical results obtained from the commercial FE/BE Sysnoise method indicated the contribution of the bending mode to the pressure was far less significant with the radiation patterns often being closer to that from a dipole force, even though the same numerical model gave excellent agreement with axial forcing. These results have not been presented here, as the discrepancy is unresolved. However, similar work conducted at the University of New South Wales (Peters *et al.* 2014) shows some similarity with the analytical results presented here. Peters *et al.* (2014) modelled a submerged hull using a fully coupled FE/BE model. They applied uniform vertical and transverse forces on the hull, and found that the peaks of radiated sound resulting from the vertical and transverse forces were primarily due to the beam bending mode of the hull. The work conducted by Peters *et al.* (2014) was validated by Qu *et al.* (2015) using a semi-analytical method. Thus, the investigation of the importance of the bending mode on the far-field sound radiation needs to be examined in future work.

6 CONCLUSIONS

An analytical method has been developed for predicting far-field sound radiation from a submerged cylindrical enclosure under arbitrary force excitations. The enclosure consists of a cylindrical shell with internal bulkheads and ring stiffeners, closed at the ends by two circular plates. An arbitrary point force can be decomposed into three orthogonal forces. The three orthogonal forces used here were in the radial, axial and tangential directions

applied to the edge of the shell on the shell-plate boundary. The expressions for the far-field sound pressure resulting from the finite shell, finite end plates and entire enclosure due to the arbitrary force excitations were given. The MATLAB code for the analytical model typically takes only 50 seconds for a complete set of solutions.

It was found that the effect of the tangential force excitation on the far-field sound pressure could be significant at some observation points. For the enclosure with a flexible shell and flexible end plates, the pressures from the shell and from the end plates could be comparable. The importance of the bending and breathing modes of the shell on the sound radiation in the far field was observed. The influence of the ring stiffeners and bulkheads on the structural response was discussed. The stiffeners were observed to have a mass effect at low frequencies and a stiffening effect at higher frequencies. The bulkheads did not have a significant effect on the enclosure driving-point responses considered in this paper.

Some verification of the analytical method is presented by using a commercial FE/BE Sysnoise method. Excellent agreement is obtained between the two methods for axisymmetric axial excitation, although some unresolved discrepancies for radial and tangential results remain. Note, however, that the numerical modelling is over 10000 times slower than computation using the analytical method.

ACKNOWLEDGEMENTS

The authors would like to thank Dr Paul Dylejko and Professor Nicole Kessissoglou for their useful discussions and suggestions.

REFERENCES

- Caresta, M. and Kessissoglou, N. 2009. 'Structural and acoustic responses of a fluid-loaded cylindrical hull with structural discontinuities'. *Applied Acoustics* **70** (2009), 954-963.
- Hopmann, II W.H. 1958. 'Some characteristics of the flexural vibrations of orthogonally stiffened cylindrical shells'. *Journal of Acoust Soc Am*, **30**, 77-82.
- Junger, M.C. and Feit, D. 1986. *Sound, Structures, and Their Interaction*. 2nd ed. An MIT Press Classic, Boston, 16-312.
- Laulagnet, B. and Guyader, J.L. 1990. 'Sound radiation by finite cylindrical ring stiffened shells'. *Journal of Sound and Vibration* **138**, 173-191.
- McLachlan, N.W. 1954. *Bessel Functions for Engineers*. Oxford University Press, London
- Pan, X. and Hansen, C.H. 1997. 'Active control of vibration transmission in a cylindrical shell'. *Journal of Sound and Vibration* **203**, 409-434.
- Pan, X., Tso, Y. and Juniper, R. 2008a. 'Active control of low-frequency hull-radiated noise'. *Journal of Sound and Vibration* **313**, 29-45.
- Pan, X., Tso, Y. and Juniper, R. 2008b. 'Active control of radiated pressure of a submarine hull'. *Journal of Sound and Vibration* **311**, 224-242.
- Peters, H., Kinns, R. and Kessissoglou, N. 2014. 'Effects of internal mass distribution and its isolation on the acoustic characteristics of a submerged hull'. *Journal of Sound and Vibration* **333**, 1684-1697.
- Scott, J.F.M. 1988. 'The free modes of propagation of an infinite fluid-loaded thin cylindrical shell'. *Journal of Sound and Vibration* **125**, 241-280.
- Skelton, E.A. and James, J.H. 1997. *Theoretical Acoustics of Underwater Structures*. Imperial College Press, London.
- Tso, Y. and Hansen, C.H. 1995. 'Wave propagation through cylinder / plate junctions'. *Journal of Sound and Vibration* **186**, 447-461.
- Qu, Y., Hua, H. and Meng, G. 2015. 'Vibro-acoustic analysis of coupled spherical-cylindrical-spherical shells stiffened by ring and stringer reinforcements'. *Journal of Sound and Vibration* **355**, 345-359.